



HAL
open science

New Mn(III) complexes with tetradentate cis-N₂O₂, acacen-type ligands. Synthesis and characterization, single-crystal X-ray diffraction and DFT studies

D. Villaman, W.A. Rabanal-León, M. Fuentealba, O. Pena, Y. Moreno

► To cite this version:

D. Villaman, W.A. Rabanal-León, M. Fuentealba, O. Pena, Y. Moreno. New Mn(III) complexes with tetradentate cis-N₂O₂, acacen-type ligands. Synthesis and characterization, single-crystal X-ray diffraction and DFT studies. *Inorganica Chimica Acta*, 2023, 555, pp.121562. 10.1016/j.ica.2023.121562 . hal-04123817

HAL Id: hal-04123817

<https://hal.science/hal-04123817>

Submitted on 21 Jun 2023

HAL is a multi-disciplinary open access archive for the deposit and dissemination of scientific research documents, whether they are published or not. The documents may come from teaching and research institutions in France or abroad, or from public or private research centers.

L'archive ouverte pluridisciplinaire **HAL**, est destinée au dépôt et à la diffusion de documents scientifiques de niveau recherche, publiés ou non, émanant des établissements d'enseignement et de recherche français ou étrangers, des laboratoires publics ou privés.



Distributed under a Creative Commons Attribution - NonCommercial 4.0 International License

“New Mn(III) complexes with tetradentate *cis*-N₂O₂, acacen-type ligands. Synthesis and characterization, single-crystal X-ray diffraction and DFT studies”

**David Villaman,^{a*} Walter A. Rabanal-León,^{a,b} Mauricio Fuentealba,^{c*} Octavio Peña,^d
Yanko Moreno^e**

^a *Laboratorio de Química Inorgánica y Organometálica, Departamento de Química Analítica e Inorgánica, Facultad de Ciencias Químicas, Universidad de Concepción, Edmundo Larenas 129, Casilla 160-C, Concepción, Chile.*

^b *Laboratorio de Modelamiento Computacional en Sistemas Inorgánicos y Organometálicos (Lab-MCSIO), Departamento de Química Analítica e Inorgánica, Facultad de Ciencias Químicas, Universidad de Concepción, Edmundo Larenas 129, Casilla 160-C, Concepción, Chile.*

^c *Laboratorio de Cristalografía, Instituto de Química, Pontificia Universidad Católica de Valparaíso, Avenida Universidad 330, Curauma, Valparaíso, Chile.*

^d *Institut des Sciences Chimiques de Rennes, UMR 6226, Université de Rennes-1, Rennes, France.*

^e *Facultad de Ciencias, Departamento de Química, Universidad de La Serena, La Serena, Chile.*

Corresponding author

David Villaman: dvillaman@udec.cl

Mauricio Fuentealba: mauricio.fuentealba@pucv.cl

Abstract

One of the challenges of manganese(III) magnetochemistry is the design and synthesis of new building block systems to study and develop molecular magnets. In this context, two new Mn(III) complexes were synthesized using new tetradentate *cis*-N₂O₂ acacen ligands from the condensation of 1-anisyl-1,3-butanedione and 1,2-diaminoethane (2:1 ratio). All compounds were fully characterized by conventional spectroscopic techniques, such as FT-IR, HRMS, and UV-Vis, and rationalized with DFT and TD-DFT studies. The resulting cationic complexes were composed of N₄O₂ coordination spheres using a tetradentate ligand (N₂O₂²⁻) in the equatorial plane and two axial pyridines with general formulae as [Mn^{III}(L)(Py)₂](X) (X = BF₄⁻; ClO₄⁻). Single-crystal X-ray diffraction revealed that both complexes are isostructural with typical axial anisotropy due to the Jahn-Teller effect by tetragonal distortion. A complete analysis of the crystalline structures revealed a nonclassical intermolecular interaction of C-H...F and C-H...O. Supported by Hirshfeld surfaces and 2D- fingerprint plots, it was possible to isolate and calculate the contribution of intermolecular interactions in the supramolecular arrangement. For both complexes, the magnetic susceptibility confirmed a high spin state (HS) with 4.8 μ_B and 4.9 μ_B related to the spin-only contribution to the magnetic moment.

Keywords: Manganese(III), Jahn-Teller, High-Spin, Uniaxial Anisotropy, Tetradentate N₂O₂ Schiff Base.

1. Introduction

Mn(III) chemistry has been widely studied in several research areas due to its synthetic facility and different properties. It has potential applications in biochemistry and biological systems, such as photosystem II [1,2], redox function as superoxide dismutase (MnSODs) [3], ribonucleotide reductase [4,5], enzymatic activity [6–8], catalysis [9–12], molecular magnetism [13–15] and single molecule magnets (SMMs) [16,17]. On the other hand, rare and recent reports have been published on the spin-crossover (SCO) phenomenon with *trans*-N₄O₂ coordination spheres using hexadentate Schiff base ligands [18–20] and single ion magnets (SIMs) with tridentate Schiff base ligands [21].

The chemistry of Mn(III) complexes is strongly related to their magnetic properties. Most of these compounds have a spin-only contribution in the high-spin state (HS) of $4.89 \mu_B$ ($S = 2$ and $g = 2.00$) at room temperature and the low-spin state (LS) of $2.83 \mu_B$ ($S = 1$ and $g = 2.00$) at cryogenic temperatures. At low temperatures, there is a decrease in the magnetic moment. This sharp drop may be due, in the case of high-spin Mn(III) complexes, to a second-order spin-orbit coupling called zero-field splitting (ZFS) of their ground state and/or to a transition from free to paired spins (antiferromagnetic alignment), to which paramagnetic impurities must be added [22,23]. The Jahn-Teller (J-T) effect generates a tetragonal distortion ($O_h \rightarrow D_{4h}$ symmetry) in an idealized octahedron geometry; therefore, the 5E_g degenerate orbital [22] is split into ${}^5B_{1g}$ and ${}^5A_{1g}$ [13–15]. The axial elongation or tetragonal elongation results in ${}^5B_{1g}$ as the ground state, where a negative zero-field-splitting D parameter is present in most cases. This feature indicates a large energy barrier to the magnetization reversal process according to the $M_s = \pm 2$ or 0 states [24,25]. Several complexes with N_4O_2 coordination spheres have been well studied in this context using salen-type ligands due to their versatility and synthetic feasibility [13,26]. One of the first reports of magnetic properties and ZFS was described in 1985 using salen tetradentate ligands [23]. For these reasons, many Mn(III) Schiff base complexes have been studied for their ferromagnetic and antiferromagnetic properties [13–15,27]. In general, a planar conformation of the tetradentate ligand leads to a uniaxial direction of the J-T effect in Mn(III), i.e., the anisotropy is localized in the dz^2 orbital. This anisotropy has been studied between two or more Mn(III) ions in dimeric complexes [28] and 1D-coordination polymers with weak or significant antiferromagnetic coupling [29,30]. The design and rational use of tetradentate ligands allow them to be used as “building blocks” for mononuclear systems, dimers, and coordination polymers. [31,32].

The magnetic properties using tetradentate ligand derivatives from β -diketones and the appropriate diamine have been studied to a lesser extent, where one of the approaches has employed Fe(III) coordination polymers [33]. Moreover, ligands and complexes derived from 1-anisyl-1,3-butanodione are scarce [34,35], but there are some similarities with these compounds previously reported, for example, in terms of keto-enamine tautomerism. Based

on this background, we report two new Mn(III) complexes with organic tetradentate ligands derived from anisole-substituted β -diketones (1-anisyl-1,3-butanedione). All compounds were fully characterized by spectroscopic techniques (FT-IR, HRMS, UV-vis), structural analysis with single-crystal X-ray diffraction (SC-XRD), magnetic susceptibility (SQUID), DFT and TD-DFT studies.

2. Experimental

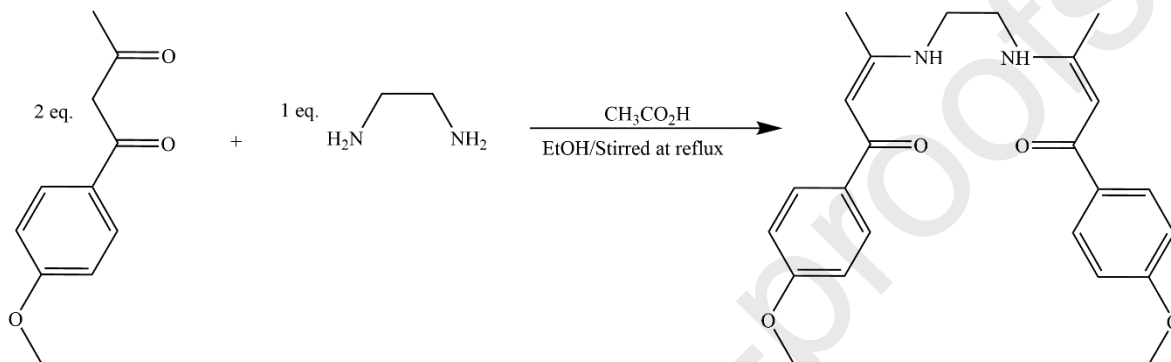
2.1 Material and methods

All reagents and solvents were obtained from Sigma-Aldrich and Merck with analytical and technical grades. To synthesize the compounds, dichloromethane and methanol solvents were used without further purification. The pyridine reagent was purchased from Sigma-Aldrich as ReagentPlus® $\geq 99\%$. Infrared spectroscopy (FT-IR) was recorded in the range of 4000–400 cm^{-1} on a Perkin-Elmer spectrometer, model Spectrum One 1600 (Figures S1-S3). The electronic spectra were measured on a Shimadzu UV-1800 spectrophotometer using a CH_2Cl_2 solution at 20 °C. The nuclear magnetic resonance spectra (RMN- ^1H ; ^{13}C) were recorded on a Bruker spectrometer, Advance 300 model (Figures S4-S5). The signals were recorded at 300 MHz for ^1H and 75 MHz for ^{13}C at 298 K. The chemical displacements are in ppm (δ) to tetramethylsilane (TMS) from the residual chemical shift of deuterated solvent (CDCl_3). High-resolution mass spectra (HRMS) were collected at the *Laboratorio de Servicio de Espectrometría de Masas (Pontificia Universidad Católica de Chile)* with a Bruker compact QTOF MS (Figures S6-S8).

2.2 Synthesis of the H₂L tetradentate ligand

1-anisyl-1,3-butanedione was added to a round bottom flask (0.5 mmol) with 1,2-diaminoethane (0.25 mmol). Then, two drops of glacial acetic acid were added to the ethanolic solution (20 mL). The reaction was stirred to reflux for thirty minutes, resulting in a microcrystalline white solid (Scheme 1). The solid was filtered and washed three times with diethyl ether, and finally, the solvent was removed under vacuum, affording the respective tetradentate ligand. **Yield:** 80%. **m.p:** 171 °C. **FT-IR (KBr pellet, $\nu_{\text{max}}/\text{cm}^{-1}$):** 3447(w) $\nu(\text{N-H})$, 3067(w), 3019(w) $\nu(\text{C-H, aryl})$, 2917(w), 2841(w) $\nu(\text{CH, alkyl})$, 1598(vs), 1582(vs), 1542(s), 1504(s) $\nu(\text{C=O})$, $\nu(\text{C-N})$ and/or $\nu(\text{C=C})$, 1179(s) $\nu(\text{C-O})$. **RMN ^1H (300**

¹H NMR, CDCl₃, δ ppm): 2.04 (s, 3H, CH₃), 3.54-3.52 (s, 2H, CH₂), 3.83 (s, 3H, OCH₃), 5.65 (s, 1H, CH=C), 6.91-6.88 (d, *J* = 8.6 Hz, 2H, 4-C₆H₄-OCH₃), 7.84-7.82 (d, *J* = 8.6 Hz, 2H, 4-C₆H₄-OCH₃), 11.46 (s, 1H, NH). **RMN ¹³C (75 MHz, CDCl₃, δ ppm):** 19.40 (CH₃), 43.90 (CH₂), 55.44 (OCH₃), 92.49 (CH=C), 113.52 (CH, 4-C₆H₄-OCH₃), 128.88 (CH, 4-C₆H₄-OCH₃), 132.89 (C_{ipso}, 4-C₆H₄-OCH₃), 161.86 (C_{ipso}, C-NH), 164.30 (C_{ipso}, 4-C₆H₄-OCH₃), 187.58 (C=O). **H RMS *m/z* (%):** 409.21 (100) [C₂₄H₂₈N₂O₄ + H]⁺.



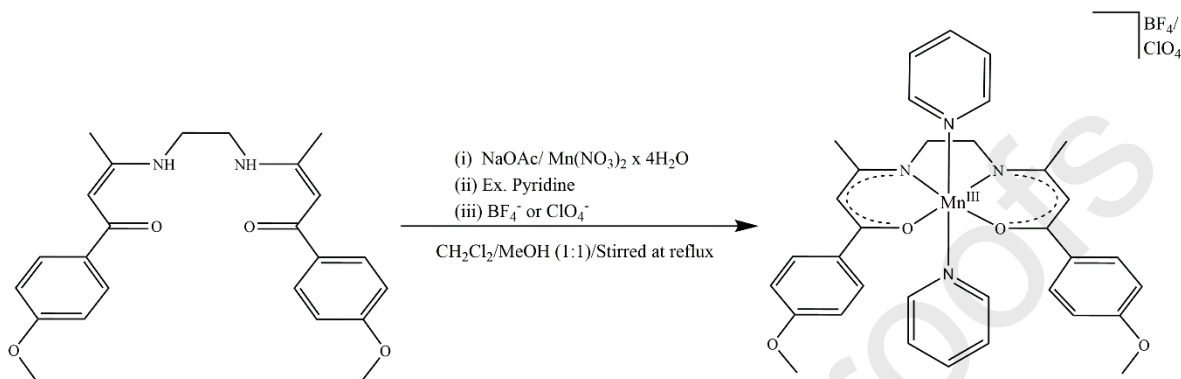
Scheme 1: Synthesis of the **H₂L** tetradentate ligand

2.3 General synthesis of complexes [Mn^{III}(L)(Py)₂](X)

H₂L was dissolved in a round bottom flask equipped with a cooling tube (0.25 mmol) in 10 mL of CH₂Cl₂/MeOH (1:1 ratio). Subsequently, sodium acetate (1 mmol) was added, and the solution was stirred to reflux for one hour. Mn(NO₃)₂ · 4 H₂O (0.28 mmol) was used, obtaining a red-colored solution after stirring for one hour. Finally, the resulting mixture was treated with an excess of pyridine (100 mmol), turned into a dark red solution, and refluxed for two additional hours. In the final solution, the counterion was added as sodium salts (BF₄⁻ and ClO₄⁻) (0.28 mmol) and then filtered with celite (Scheme 2). The filtered solution was allowed to crystallize for several days by slow evaporation, affording dark red block-shaped single crystals.

[Mn^{III}(L)(Py)₂](BF₄): Yield: 38%. **FT-IR (KBr pellet, ν_{max}/cm⁻¹):** 1603 (s), 1588 (s), 1569 (m) ν(C···O), ν(C···N) and/or ν(C···C), 1030(m) ν(BF₄). **HRMS *m/z* (%):** 461.13 (81) [Mn^{III}(L)]⁺, 622.03 (3.5) [Mn^{III}(L)(Py)₂ + H]⁺.

[Mn^{III}(L)(Py)₂](ClO₄): Yield: 36%. FT-IR (KBr pellet, $\nu_{\max}/\text{cm}^{-1}$): 1604(s), 1585(s), 1587(m) $\nu(\text{C}\cdots\text{O})$, $\nu(\text{C}\cdots\text{N})$ and/or $\nu(\text{C}\cdots\text{C})$, 1098(s) and 622(m) $\nu(\text{ClO}_4)$. HRMS m/z (%): 461.13 (28) [Mn^{III}(L)]⁺, 622.03 (5.7) [Mn^{III}(L)(Py)₂ + H]⁺.



Scheme 2: General synthesis of the complexes [Mn^{III}(L)(Py)₂](X).

2.4 Single-crystal X-ray diffraction

Diffraction data were collected on a Bruker D8 QUEST diffractometer equipped with a two-dimensional CMOS Photon 100 detector using Mo-K α (0.71073 Å) radiation. The tetradentate ligand was collected at 298 K, whereas the complexes [Mn^{III}(L)(Py)₂](X) were measured at 170 K. The patterns were integrated with the APEX3 package and the absorption correction of the complexes with SADABS [36]. The structures were solved with the intrinsic phasing method using ShelXT [37] and later refined with full-matrix least-squares methods based on F^2 ShelXL [38] using OLEX2 software version 1.3 [39]. All the atoms were refined with anisotropic parameters except for the hydrogen atoms that were calculated and refined from isotropic thermal parameters with riding coordinates. All groups CH, CH₂, and NH were set with a Uiso value equal to 1.2x, and the hydrogen atoms of the CH₃ group were set with Uiso at 1.5x. (Tables S1- S8).

(CCDC deposition numbers 2240292 for **H₂L**, 2240293 for [Mn^{III}(L)(Py)₂](BF₄) and 2240294 for [Mn^{III}(L)(Py)₂](ClO₄) contain the crystallographic data for this paper).

2.5 Hirshfeld surface analysis

The Hirshfeld surfaces and 2D- fingerprint plots [40–42] were generated and calculated with the Crystalexplorer program [43]. The crystallographic information file (CIF) was used as the input file for each complex. The Hirshfeld isosurfaces were mapped using the normalized contact distance (d_{norm}) defined by d_e , d_i and r^{vdW} according to

$$d_{norm} = \frac{(d_i - r_i^{vdW})}{r_i^{vdW}} + \frac{(d_e - r_e^{vdW})}{r_e^{vdW}}$$

The terms d_e and d_i are the distances from the isosurface to the nearest external (outside of surface) and internal (inside of the surface) nucleus, respectively, and r^{vdW} is the van der Waals radii (vdW) of the atoms in the molecule. The value of d_{norm} is represented by three colors on the surface: red, blue, and white, where a red spot is defined as the shortest contact than the sum of van der Waals radii, a blue spot is the longest contact, and the white color is representative around the sum of the vdW separation. 2D-fingerprint plots were used to analyze the contribution of each intermolecular interaction in the crystal, and the Hirshfeld surface was mapped and plotted as d_e versus d_i .

2.6 Powder X-ray diffraction

The X-ray powder diffractograms were collected at 298 K on a Bruker D8 diffractometer Advance equipped with a LINKEYE 0D detector using a Cu-K α (1.5406 Å) radiation source. The samples were studied in the range of $2\theta = 10\text{--}50^\circ$. Therefore, these patterns were compared and overlapped with the single-crystal X-ray diffraction data generated by Mercury software [44]. (Figures S9-S10).

2.7 Magnetic experiments

The magnetic data of the $[\text{Mn}^{\text{III}}(\text{L})(\text{Py})_2](\text{X})$ complexes were recorded on a SQUID magnetometer, Quantum Design brand, and MPMS-XLS5 model. The magnetic susceptibilities were corrected by the diamagnetic contributions of the samples, calculated from the Pascal constants [45], and the contribution of the sample carrier was measured separately. Finally, approximately 6.5 and 6.1 milligrams of the complexes were measured with an external field of 500 Oe as a function of the temperature in ZFC/FC modes from 2–330 K.

2.8 Computational details

All the calculations were carried out using Gaussian 16 software. The computational model was built considering the single-crystal X-ray diffraction (SC-XRD) data from the experimental section without the tetrafluoroborate and/or perchlorate counterions. The previously mentioned model of the $[\text{Mn}^{\text{III}}(\text{L})(\text{Py})_2]^+$ complex ion was fully optimized at the DFT level by using the PBE0 [46,47] hybrid exchange-correlation (XC) functional in conjunction with a triple-zeta quality basis set def2-TZVP that includes relativistic corrections by using the Ahlrichs effective core potential [48]. The optimized structure was confirmed as local minima via numerical frequency analysis. This frequency analysis also contributes to supporting the FT-IR spectrum assignments using potential energy distribution (PED) analysis as implemented in the VEDA4xx code [49] (suggested by the author for molecules larger than 20 atoms).

The previous methodology was validated based on the structural determinations between crystallographic data and the DFT-optimized model for the $[\text{Mn}^{\text{III}}(\text{L})(\text{Py})_2]^+$ ion. In this case, the optimized structure was merged with the respective molecular structure from SC-XRD, and then a root-mean-square deviation (RMSD) analysis was performed using Chemcraft visualization software [50].

Additionally, the UV–Vis spectrum was calculated using the TD-DFT approach [51]; excitation energies and oscillator strength intensities were computed at the same level of theory as in the DFT calculations [52]. Furthermore, the molecular orbital composition of the main electronic transitions was analyzed to provide band assignments of the

experimental UV–Vis spectrum. Solvent effects were introduced into the excitation energy calculations using a polarizable continuum model (PCM) using dichloromethane as an implicit solvent [53,54].

3. Results and Discussion

3.1 Crystallographic studies of the **H₂L** tetradentate ligand

The **H₂L** tetradentate ligand crystallizes into a *P*-1 triclinic space group, with one molecular entity per unit cell (*Z*=1). In Table 1, the bond distances and angles are detailed, where the mean plane is defined considering atoms O1-C8-C9-C10-N1 (Figure 1). The angles between O1-C8-C9, C8-C9-C10 and C9-C10-N1 are 123.07(14)°, 124.47(13)°, and 121.65(14)°, respectively, suggesting *sp*² hybridization for carbon atoms. On the other hand, the bond length for the same plane suggests a delocalized system between C8 and N1, but the most significant difference occurred along the bond C8=O1, which has a double bond character [55,56]. This antecedent could suppose that the major contribution is from the keto-enamine tautomer rather than the keto-imine or enol-imine tautomer. Tridentate ligands derived from 1-anisyl-1,3-butanedione have been previously reported [34,35,57], and the structural analysis has revealed a keto-enamine or enaminone tautomerism, which agrees with the distances and angles reported for the **H₂L** ligand.

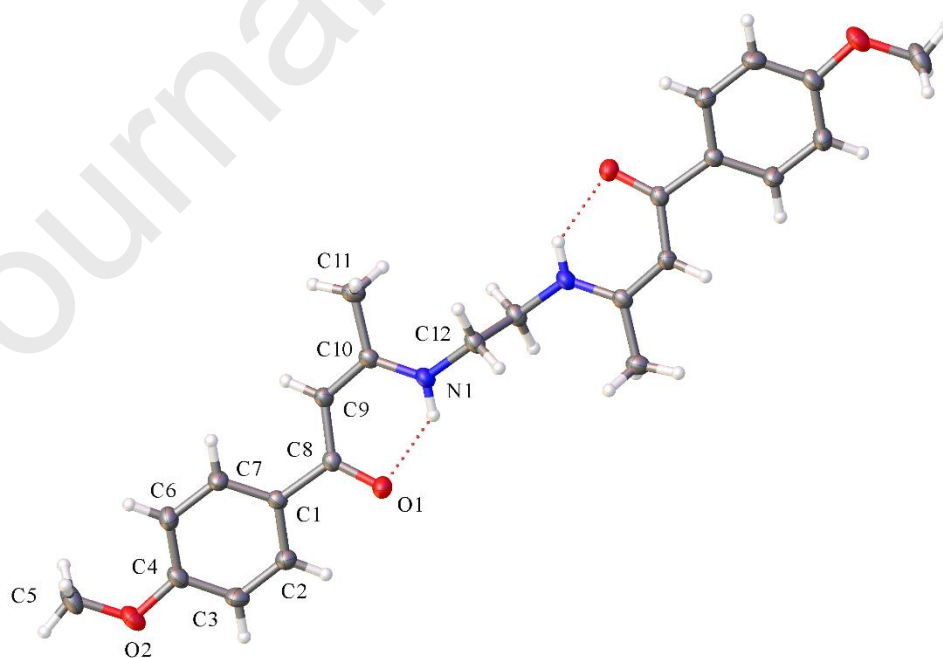


Figure 1: ORTEP plot of the **H₂L** tetradentate ligand. A thermal ellipsoid was drawn with a 30% probability.

Table 1: Bond distances and angles of the **H₂L** tetradentate ligand

Space Group		<i>P</i> -1	
T/K		298	
Bond distances/Å			
C1-C8	1.5012(19)	C3-C4	1.377(2)
C8-O1	1.2523(18)	C4-O2	1.3642(19)
C8-C9	1.414(2)	C5-O2	1.423(2)
C9-C10	1.382(2)	C4-C6	1.370(2)
C10-N1	1.3318(19)	C6-C7	1.388(2)
C10-C11	1.494(2)	C1-C7	1.377(2)
C1-C2	1.387(2)	C12-N1	1.4550(18)
C2-C3	1.378(2)	C12-C12ⁱ	1.522(3)
Bond angles/°			
C1-C8-O1			117.71(13)
C9-C8-O1			123.07(14)
C8-C9-C10			124.47(13)
C9-C10-N1			121.65(14)
C11-C10-N1			118.87(13)
C12ⁱ-C12-N1			112.16(16)
Plane¹-plane²			18.11(7)

Symmetry code: $\bar{1}$ -x, 2-y, 1-z

Abbreviation: Plane¹: O1-C8-C9-C10-N1; Plane²: C1-C2-C3-C4-C6-C7

The dihedral angle between the plane formed by O1-C8-C9-C10-N1 (Plane¹) and the plane composed of C1-C2-C3-C4-C6-C7 (Plane²) was 18.12(7)°. In addition, the ligand contained an intramolecular hydrogen bond (Table 2) from the amine proton to carbonyl oxygen, closing a pseudoaromatic ring of six members [58–60] (Figure 1).

Table 2: Bond distances and angles (Å, °) by the intramolecular hydrogen bond

<i>D-H...A</i>	<i>D-H</i>	<i>H...A</i>	<i>D...A</i>	<i>D-H...A</i>
N1-H1... O1	0.86	2.01	2.6842(16)	134.4

3.2 Crystallographic studies of the [Mn^{III}(L)(Py)₂](X) complexes

The crystallographic details of the complexes are listed in supporting information Tables S4-S5. The Mn(III) complexes crystallized in the *P*-1 triclinic space group with two formula units per unit cell (*Z* = 2). The complexes were coordinated by the N₂O₂²⁻ organic tetradentate ligand as the equatorial plane and two pyridine molecules in the axial position. Each complex was cationic with tetrafluoroborate and perchlorate anions (X = BF₄⁻; ClO₄⁻) described as [Mn^{III}(L)(Py)₂](X) (Figures S11 and S12).

The axial anisotropy along the Mn1-N3 and Mn1-N4 bonds was the largest variation observed within the coordination sphere by tetragonal distortion due to the Jahn-Teller effect (J-T) in Mn(III) [13]. The bond distances from the *cis*-N₂O₂ equatorial plane were in agreement with Mn(III) acacen complex derivatives [61,62]. The octahedral deviation parameters from Σ /° [63] ($\Sigma = \sum_{i=1}^{12} |\varphi_i - 90|$) were 22.1(2)° and 22.5(3)° for [Mn^{III}(L)(Py)₂](BF₄) and [Mn^{III}(L)(Py)₂](ClO₄); moreover, the Θ /° [64] parameters ($\Theta = \sum_{i=1}^{24} |\theta_i - 60|$) were 119.0(3)° and 118.6°(3), respectively, which were smaller than those of polymeric salen analogs [65,66].

In the aliphatic bridge, the C12 and C24 carbon atoms were deflected by +0.206(3) Å and -0.275(3) Å from the (N1-Mn1-N2) plane (Figure S13), respectively. The deviations mentioned above have been observed for Fe(III) SCO complexes [Fe^{III}(acen)(bpp)](BPh₄) [67,68] and [Fe^{III}(acen)(tmid)](BPh₄) [68] using acacen ligands. Ross [33] *et al.* described this conformation as *meso* type by symmetric variation of the amine carbons (C10 and C22) above and below the N₂O₂ plane.

On the axial axis, the same pyridine arrangement was observed in both complexes. In fact, the plane formed by (C25-C26-C27-C28-C29-N3) was practically aligned to the axis composed of N1-Mn1-O3 (Figure 2). In contrast, the opposite pyridine (C30-C31-C32-C33-C34-N4) was slightly aligned to the N2-Mn1-O1 axis. This arrangement was different compared to salen and/or acacen complexes with a *meso* conformation [26,67]. Finally, the dihedral angle ($\approx 20^\circ$) between aromatic rings A and B (Figure 2) and the N₂O₂ plane may be due to hydrogen bond contact (see below) with the anisyl moieties.

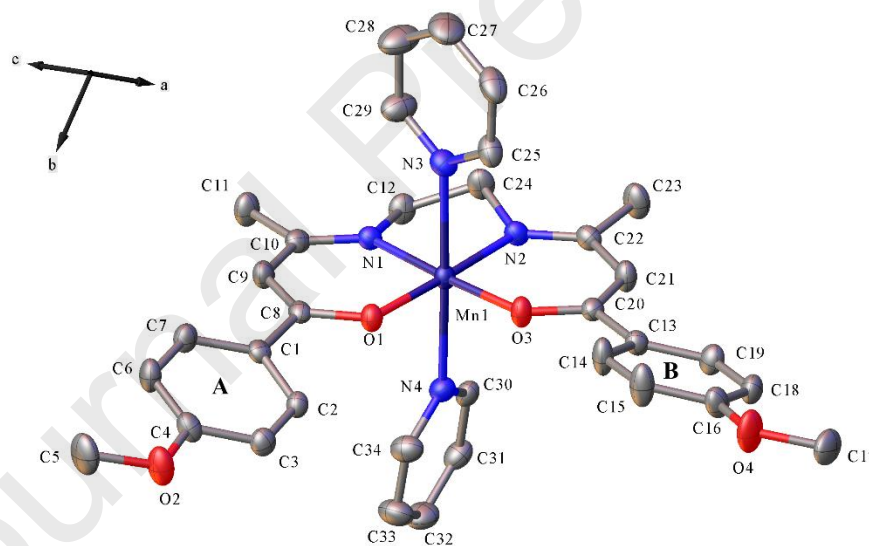


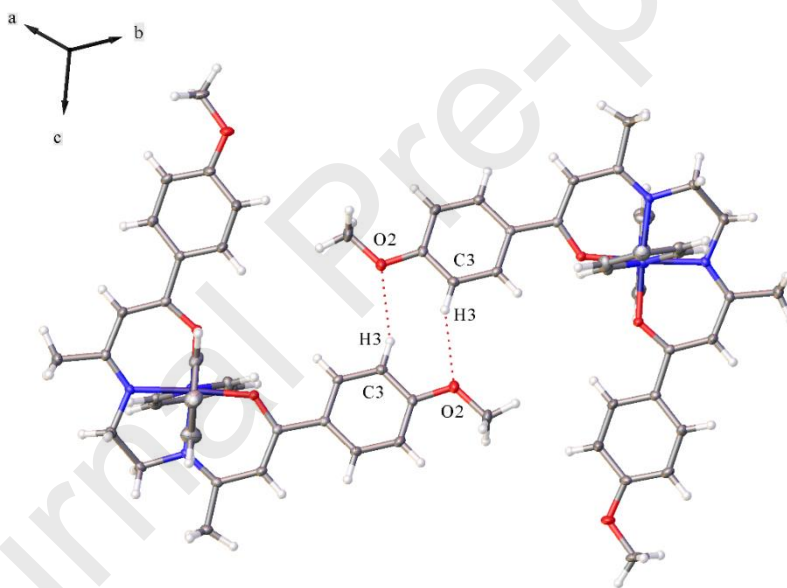
Figure 2: ORTEP of [Mn^{III}(L)(Py)₂](BF₄) and anisole rings A and B. A thermal ellipsoid was drawn with 30% probability. Hydrogen atoms were omitted for the sake of clarity.

3.3 Crystalline structure and Hirshfeld surfaces

At the supramolecular level, the crystal packing revealed π - π stacking interactions between axial pyridine ligands. The π - π contacts were formed between the plane (C25-C26-C27-

C28-C29-N3) and the adjacent plane (C25-C26-C27-C28-C29-N3) $(-x, 1-y, 1-z)$ by parallel displacement [69]. (Figure S14).

Nonclassical hydrogen bonds were found as C-H \cdots F and C-H \cdots O contacts. In both complexes, it is possible to find intra- and intermolecular interactions generated by counterions, and those contacts can be described with the graph set *motif* $D_1^1(2)$ as dimers. Despite the influence of counterions, there are two intermolecular interactions, C3-H3 \cdots O2 $(-x, 2-y, 1-z)$ and C33-H33 \cdots O4 $(1-x, 2-y, 1-z)$, which can be described with the graph set *motif* $R_2^2(8)$ and $R_2^2(24)$ as a ring (Figure 3). These arrangements are related to the methoxy group (O-CH₃) described in supramolecular structures [70–72]. The *bc* plane (Figure S15) displays the distribution of hydrogen bonds due to the influence of the counterion and methoxy groups.



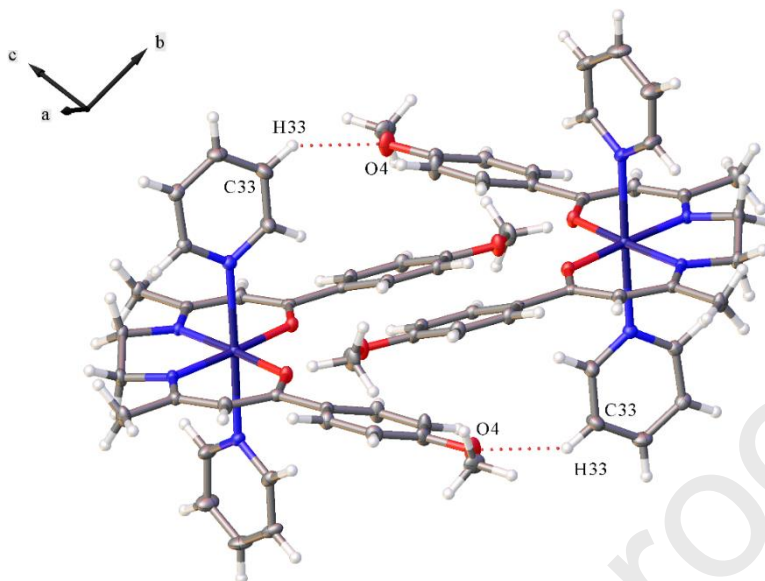


Figure 3: The C3-H3 \cdots O2 and C33-H33 \cdots O4 intermolecular hydrogen bonds of [Mn^{III}(L)(Py)₂](BF₄). The tetrafluoroborate counterion was omitted for the sake of clarity.

Hirshfeld surfaces [42] were generated to analyze the intermolecular interactions in the crystalline packing. In Figure 4, the surfaces were mapped as d_{norm} for each complex. A red spot on the isosurface (Figure 4) is evidence of intra- and intermolecular interactions. In addition, the fingerprints were plotted from the Hirshfeld surface information, where the relative contribution of the contacts and their crystalline pattern were exhibited. Further analysis with 2D fingerprint plots [40,41] showed the presence of nonclassical interactions, such as the C-H \cdots O and C-H \cdots F types described above. In both complexes, approximately 46% of the total Hirshfeld surface area is due to H \cdots H interatomic contacts ($d_e = d_i$). The C-H \cdots C bond was observed as a wide symmetrical wing related to the C-H \cdots π interaction [73,74] with a high contribution of 29% from the surface (Figure 5). For the [Mn^{III}(L)(Py)₂](BF₄) complex, the C-H \cdots O (O \cdots H/H \cdots O) and C-H \cdots F contacts appeared with a total contribution of 20.8% (C-H \cdots O = 8.3%; C-H \cdots F = 12.5%); however, in [Mn^{III}(L)(Py)₂](ClO₄), only the O \cdots H/H \cdots O interaction appeared with a total of 21% (Figure S16). These contributions differ significantly compared to Mn(III) dimeric complexes [8,75]. In the [Mn^{III}(L)(Py)₂](BF₄) complex (Figure 5), C-H \cdots F was asymmetrically exhibited in the scatter plot as a single contribution of tetrafluoroborate counterion due to the lack of fluorine atoms in the complex. Conversely, the reciprocal

contact of $O\cdots H/H\cdots O$ was displayed as a broad symmetrical wing. On the other hand, for $[\text{Mn}^{\text{III}}(\text{L})(\text{Py})_2](\text{ClO}_4)$, the $O\cdots H/H\cdots O$ interaction was represented as a wide asymmetrical wing due to the contribution of the perchlorate counterion (Figure S16). Finally, regarding the $\pi\text{-}\pi$ stacking interactions, the contribution of $C\cdots C$ ($\pi\cdots\pi$ type contact) represents only $\approx 1\%$ of the total surface area.

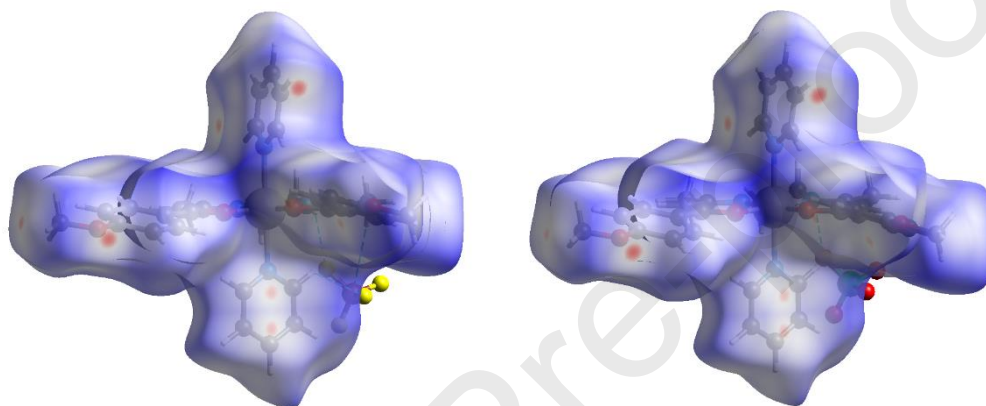


Figure 4: Hirshfeld surfaces mapped with d_{norm} over molecular structures of $[\text{Mn}^{\text{III}}(\text{L})(\text{Py})_2](\text{BF}_4)$ and $[\text{Mn}^{\text{III}}(\text{L})(\text{Py})_2](\text{ClO}_4)$ complexes.

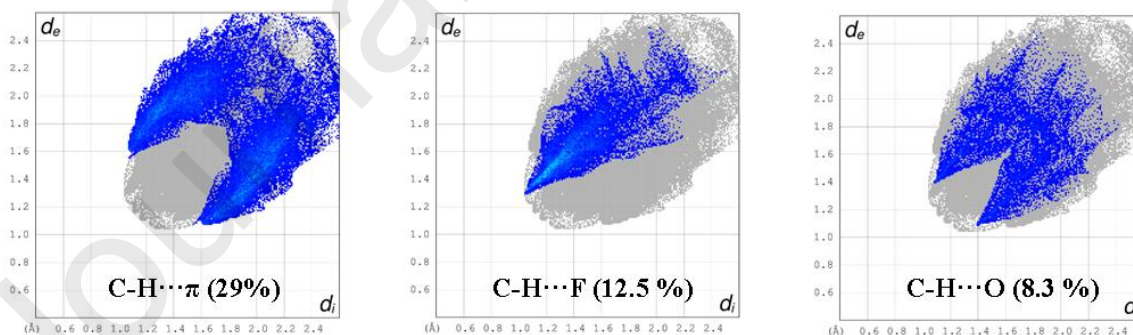


Figure 5: 2D-Fingerprint plots of $[\text{Mn}^{\text{III}}(\text{L})(\text{Py})_2](\text{BF}_4)$; $C\text{-H}\cdots\pi$, $C\text{-H}\cdots\text{O}$ and $C\text{-H}\cdots\text{F}$ interactions.

3.4 Magnetic measurements

The magnetic studies of the complexes $[\text{Mn}^{\text{III}}(\text{L})(\text{Py})_2](\text{X})$ are based on magnetic susceptibility measurements, determined as a function of temperature in the range 2–330 K. The thermal dependence of the $\chi_{\text{M}}T$ product (χ_{M} , the molar susceptibility corrected by the diamagnetic contribution) is shown in Figures 6 and S17.

The plots showed that the $\chi_{\text{M}}T$ product was stable at high temperatures but decreased abruptly below 30 K. The analysis of χ_{M}^{-1} vs. T leads (Figure S18) to magnetic moments of $4.8 \mu_{\text{B}}$ and $4.9 \mu_{\text{B}}$ for $[\text{Mn}^{\text{III}}(\text{L})(\text{Py})_2](\text{BF}_4)$ and $[\text{Mn}^{\text{III}}(\text{L})(\text{Py})_2](\text{ClO}_4)$ complexes, respectively, which was in agreement with the values expected for the $3d^4$ configuration in the HS state [22,76].

Figures 6 and S17 show that the experimental data are superimposed with those that fit a mononuclear Mn(III) model (spin-only formula). The fit curve was in agreement for both cases, and the values of g and θ were 1.98 and -1.3 K ($[\text{Mn}^{\text{III}}(\text{L})(\text{Py})_2](\text{BF}_4)$) and 1.99 and -1.89 K ($[\text{Mn}^{\text{III}}(\text{L})(\text{Py})_2](\text{ClO}_4)$), respectively.

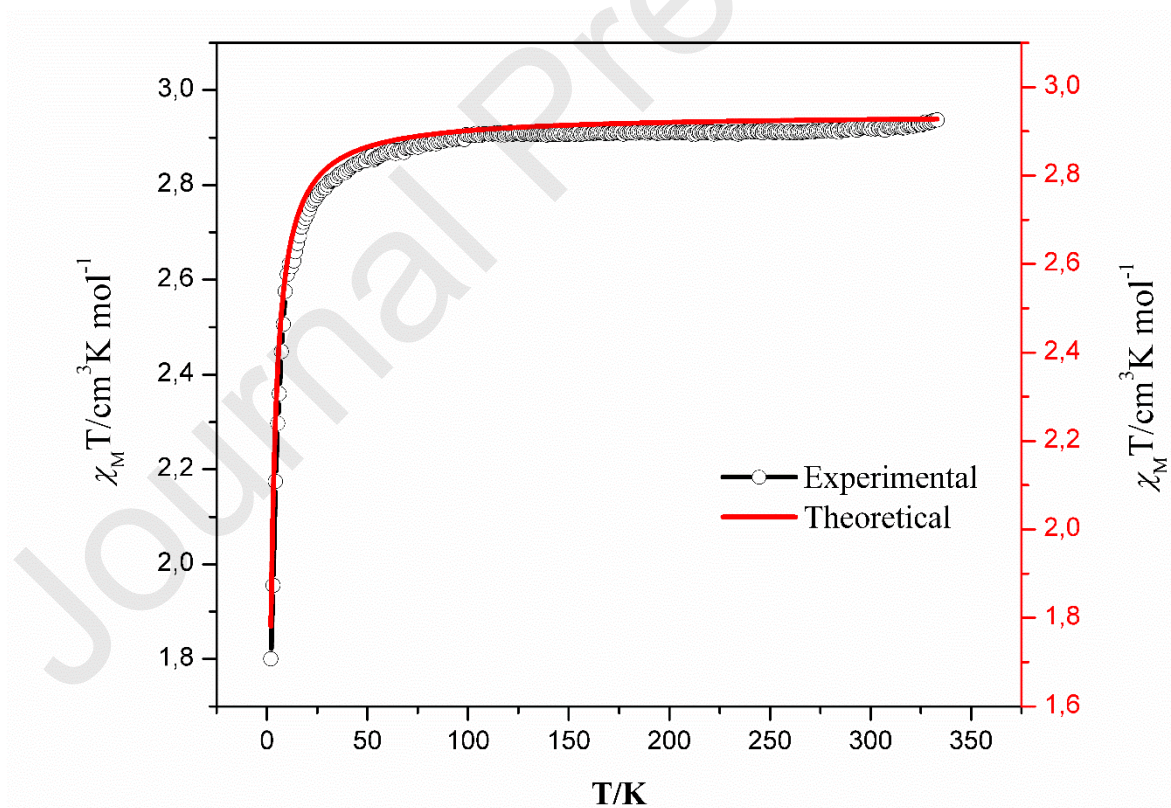


Figure 6: Magnetic susceptibilities of the $[\text{Mn}^{\text{III}}(\text{L})(\text{Py})_2](\text{BF}_4)$ complex as a function of temperature (2–330 K).

Statistical analysis, along with some quantum mechanical considerations, leads to the following Equations (1) and (2):

$$(1) \chi_A = \frac{Ng^2\beta^2}{3kT} \cdot J(J + 1)$$

Because $J = S$ is considered,

$$(2) \chi_A = \frac{Ng^2\beta^2}{3kT} \cdot 2(2 + 1)$$

Equation (2) was modified to include the value of the Curie–Weiss constant, θ . Finally, Equation (3) is given:

$$(3) \chi_A = \frac{6Ng^2\beta^2}{3k} \cdot \frac{1}{(T-\theta)}$$

For this configuration, the ground term is 5E_g from the 5D term of the free ion.

The first approximation to the E term gives no orbital contribution. However, if there is a T term of the same multiplicity at a higher energy, it is possible for spin-orbit coupling to "mix" some of this into the ground term, introducing a certain amount of orbital angular momentum into the latter. The reason is that the ligand field can quench orbital angular momentum and has no effect on spin angular momentum. Consequently, if the two are coupled by spin-orbit coupling, the ligand field is unable to affect a perfect separation of terms of the same multiplicity based on their differing orbital angular momentum. The ground term may, therefore, retain some orbital angular momentum, which is equivalent to saying that it is not a pure E term.

However, since the experimental values give a moment very close to that given by a spin-only model, the analysis was simplified with a quenching-orbital contribution. Then, Equation (4) predicts the following:

$$(4) g = 2 \cdot \left(1 - \alpha \frac{\lambda}{10Dq} \right)$$

where α is 2 for an E term, λ is related to spin-orbit coupling, and $10Dq$ is the energy separating the interacting term. Although the deviation of the expected and experimental values is not significant, for this reason, the main contribution to the magnetic moment is

the electronic spin [22]. In general, these explanations are in agreement with Mn(III) salen complexes [77,78] by spin-only contribution to the magnetic moment (orbital quenching).

3.5 UV–Vis spectroscopy

The UV–Vis spectrum for all compounds was measured from 250 to 700 nm in CH₂Cl₂ solution at 20 °C (Figures 7 and S19). The UV–Vis spectra of the **H₂L** tetradentate ligand are detailed in Figure S20. Both complexes have three experimental absorptions (Table 3). In Mn(III) complexes, the ligand field under idealized octahedral geometry is related to the $^5E_g \rightarrow ^5T_g$ transition. However, the nature of the Jahn-Teller effect generates a tetragonal distortion decreasing the symmetry; therefore, the ground term splits into $^5B_{1g}$ and $^5A_{1g}$ terms. For this reason, the spectral analysis is not quite simple, and TD-DFT studies were carried out to support the experimental data (see below). A broad band between 500 and 670 nm was observed and assigned to d-d transitions allowed by spin. These weak bands appeared at 516 and 521 nm, which was in agreement with Mn(III) Schiff base complexes [79]. Both complexes have a strong band at 416 nm related to ligand-to-metal charge transfer (LMCT), and a strong band at 317–318 nm was assumed to be the $\pi \rightarrow \pi^*$ transition [80].

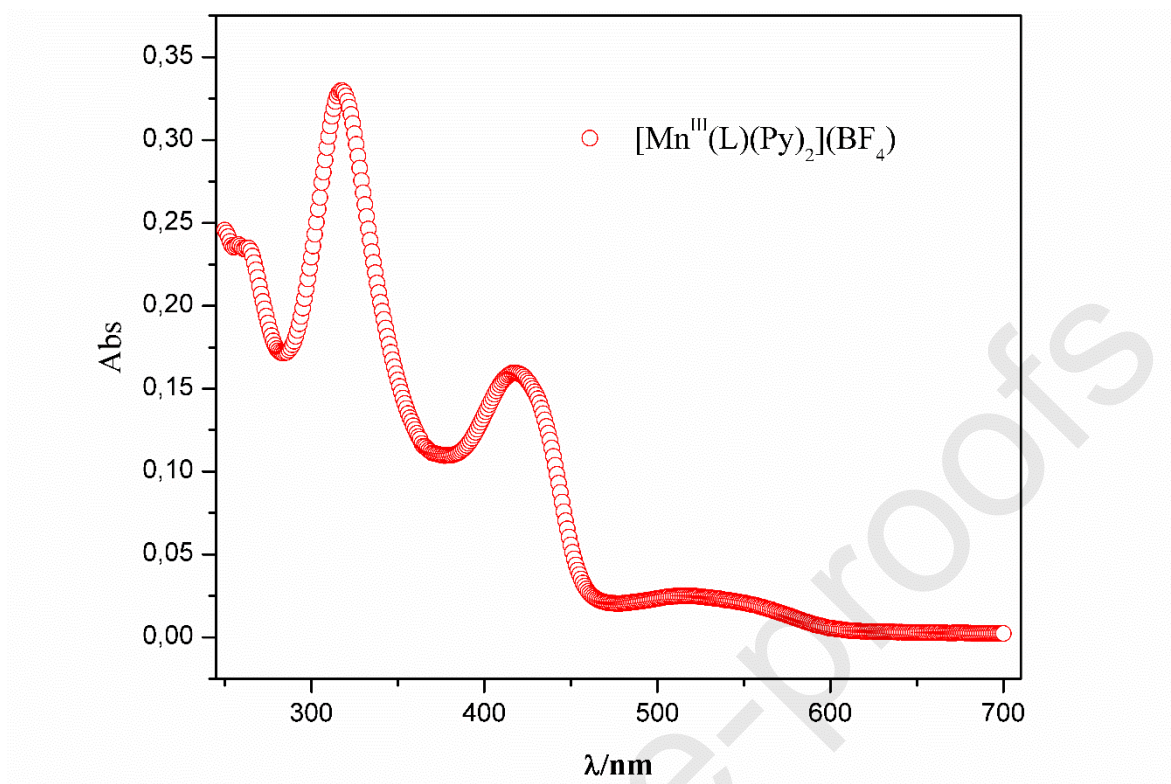


Figure 7: UV-Vis spectra of $[\text{Mn}^{\text{III}}(\text{L})(\text{Py})_2](\text{BF}_4)$ in CH_2Cl_2 at $20\text{ }^\circ\text{C}$.

Table 3: Electronic spectra data of $[\text{Mn}^{\text{III}}(\text{L})(\text{Py})_2](\text{X})$ complexes

Complexes	$\lambda_{\text{max}}/\text{nm}$ ($\log \epsilon$)
$[\text{Mn}^{\text{III}}(\text{L})(\text{Py})_2](\text{BF}_4)$	516 (2.40)
	416 (3.21)

	317 (3.52)
$[\text{Mn}^{\text{III}}(\text{L})(\text{Py})_2](\text{ClO}_4)$	521 (2.23)
	416 (3.07)
	318 (3.39)

3.6 Computational studies

Structural Analysis: Root-mean-square deviation (RMSD) analysis showed structural differences in the range of 0.558 Å, which are less than 50% of the C-H atom. The main differences in the compared structures are mainly due to the free rotation of the pyridine ligands and the peripheral phenyl-methoxy groups in the tetradentate ligand. These slight rotations do not affect the coordination environment of the manganese ion, which remains octahedral. This RMSD analysis confirms slight variations between the models and the crystallographic data. The optimized structural coordinates, the results obtained from the RMSD analysis and the merged figure of both crystal and optimized structures are shown in the supporting information (Table S9 and Figure S21).

FT-IR Analysis: The potential energy distribution (PED) analysis aims to represent all normal modes by clear internal coordinates that describe the vibrational movements of the molecule and, therefore, its FT-IR spectra. To do this, vibrational energy distribution analysis (VEDA) maximizes the elements of the PED matrix. In this matrix, the internal coordinates are in columns (Table S10), the modes are in rows, and the entries denote the percent contribution of the internal coordinate to the normal vibration mode (IR active mode). Both the maximization and optimization routines implemented in VEDA allow us to obtain a better and more accurate description of theoretical-IR results and provide a proper assignment of the FT-IR signals that can be contrasted with experimental data.

In this context, the PED contributions, mode interpretations, and mode classification are gathered in Table 4 for the $[\text{Mn}^{\text{III}}(\text{L})(\text{Py})_2]^+$ complex ion. Additionally, a schematic comparison of the calculated and experimental FT-IR spectra is depicted in Figure S22, where the results showed that the calculated FT-IR spectra are in good agreement in shape,

position, and intensity with the experimental spectra; furthermore, Table 4 reports the final set of internal coordinates for the complete set of FT-IR signals in the $[\text{Mn}^{\text{III}}(\text{L})(\text{Py})_2]^+$ complex ion.

Table 4: Selected PBE0/Def2-TZVP calculated frequencies (ν_{calc} , cm^{-1}), IR intensities (I_{IR} , km/mol), and mode assignments PED (%) for the $[\text{Mn}^{\text{III}}(\text{L})(\text{Py})_2]^+$ complex ion in contrast to experimental data (ν_{Exp} , cm^{-1}).

ν_{exp}	ν_{calc}	I_{IR}	PED	Assignment
3450	3454	3.61	S1 (35%)	ν_{CH}
1603	1677	37.72	S41 (15%)	τ_{HCOCl}
			S58 (20%)	
			S155 (18%)	
1568	1560	102.33	S41 (15%)	τ_{HCOH}
			S58 (20%)	
			S155 (18%)	
1083	1114	14.18	S66 (22%)	β_{HCC}
			S71 (12%)	τ_{HCCC}

Excitation energies and calculated UV–Vis spectra: The computed excitation energies for the $[\text{Mn}^{\text{III}}(\text{L})(\text{Py})_2]^+$ complex ion exhibit the same three bands observed experimentally (Table 5 and Table S11). Analyzing the molecular orbitals involved in the transitions, the first band (band a) can be characterized as a mix between $\pi \rightarrow \pi^*$ intraligand and LMCT excitations at 368 nm (exp. 318 nm). The second band (band b) can be characterized by excitations to two different excited states. These could be depicted as purely LMCT electronic transitions located at 404 and 418 nm (exp. 416 nm). Finally, the third band (band c) is also composed of excitations to two different excited states. However, in this case, the excitations are mainly centered on the d -orbitals of the metal ion with a small contribution from the N_2O_2 -ligand in the departure molecular orbitals and from the pyridine ligand in the arrival molecular orbitals. These small ligand contributions can be explained by the σ - and π -type delocalized electron density provided by the N_2O_2^- and pyridine ligands to the t_{2g} and e_g metal atomic orbitals, respectively. The excitations for this band can be found at 518 (exp. 516 nm) and 523 nm. This analysis allows us to confirm the initial band assignment for the coordination complex.

Table 5: Excitation energies (eV), wavelengths (nm), oscillator strengths (f), and orbital assignments for the $[\text{Mn}^{\text{III}}(\text{L})(\text{Py})_2]^+$ complex ion calculated at the PBE0/Def2-TZVP level of theory. Solvation effects were included via the PCM using CH_2Cl_2 as the solvent.

Band	Energy (eV)	λ (nm)	f (x100)	Active MOs	Percent of contribution	Assignment
a	3.36	368.9 (exp. 318)	4.46	$139\alpha \rightarrow 166\alpha$	37.5%	$\pi-\pi^*$
				$155\alpha \rightarrow 165\alpha$	17.2%	LMCT
				$157\alpha \rightarrow 165\alpha$	12.2%	LMCT
b	3.06	404.8	12.66	$158\beta \rightarrow 168\beta$	26.0%	LMCT
				$159\alpha \rightarrow 165\alpha$	14.4%	LMCT
				$158\beta \rightarrow 167\beta$	11.9%	LMCT
				$160\alpha \rightarrow 165\alpha$	26.4%	LMCT
c	2.96	418.8 (exp. 416)	0.31	$161\alpha \rightarrow 165\alpha$	15.7%	LMCT
				$160\beta \rightarrow 165\beta$	12.4%	LMCT
				$163\alpha \rightarrow 165\alpha$	11.5%	LMCT
				$162\alpha \rightarrow 165\alpha$	44.7%	d-d
c	2.39	518.7 (exp. 516)	0.58	$161\alpha \rightarrow 165\alpha$	25.1%	LMCT
				$164\alpha \rightarrow 165\alpha$	87.7%	d-d
				$163\alpha \rightarrow 165\alpha$	9.18%	LMCT

Conclusion

Two new isostructural Mn(III) complexes have been synthesized using tetradentate ligands derived from β -diketones and 1,2-diaminoethane. The organic ligand and complexes were fully characterized by conventional spectroscopic techniques (FT-IR, HRMS, UV-Vis),

single-crystal X-ray diffraction (SC-XRD), and magnetic susceptibilities (SQUID). The DFT studies by RMSD analysis confirmed slight variations of the optimized structure and the experimental model with a difference of 0.558 Å. Therefore, the crystallographic structure was in accordance with the theoretical model in the solid state. This structural analysis revealed that the most significant variations occurred in the case of the pyridines and the anisole group due to the degree of rotation. The disposition and arrangement between two axial pyridines were essentially electronic, with a contribution of p orbitals from the monodentate ligand that was supported by the TD-DFT calculations. On the other hand, the Hirshfeld surface analysis revealed nonclassical interactions of the C-H \cdots F and C-H \cdots O types, contributed mainly by the respective tetrafluoroborate and perchlorate counterions. The 2D-fingerprint plots indicated a 29% contribution of C-H \cdots π contacts, probably due to a high number of aromatic moieties in the complexes, and C \cdots C ($\pi\cdots\pi$ contact) was only 1% of the total surface, which could be mostly related to the π - π stacking of axial pyridines. At room temperature, the magnetic susceptibility revealed an HS state, which stabilized the magnetic moment with 4.8 μ_B and 4.9 μ_B values (spin-only formula). Based on the spin-only formula, the substantial drop of the magnetic moment was attributed to the second-order spin-orbit coupling as well-known zero-field-splitting (ZFS) and/or a transition from free spins to paired spins. UV-visible spectroscopy revealed a broad band between 516 and 521 nm, related to d-d transitions. These assignments were corroborated by TD-DFT analysis, which includes the bands associated with $\pi\rightarrow\pi^*$ and LMCT mixed contribution at 318 nm and purely LMCT at 416 nm. Finally, our contribution opens the door to use noncommercial β -diketones to synthesize new Mn(III) complexes that serve as building blocks for 1D polymeric systems in the search for new molecular magnets.

Acknowledgments

The authors acknowledge FONDEQUIP EQM 120095, D.I. Pontificia Universidad Católica de Valparaíso (PUCV), and the Chilean French International Research Project “IRP-CoopIC”. W.R-L., thanks the financial support from the National Agency for

Research and Development (ANID) through project N° 11190561 FONDECYT – *Iniciación en Investigación*. David Villaman, thanks to ANID FONDECYT – Postdoctoral N° 3210226.

References

- [1] V.K. Yachandra, K. Sauer, M.P. Klein, Manganese cluster in photosynthesis: Where plants oxidize water to dioxygen, *Chem. Rev.* 96 (1996) 2927–2950. doi:10.1021/cr950052k.
- [2] A. Zouni, H.-T. Witt, J. Kern, P. Fromme, N. Krauss, W. Saenger, P. Orth, Crystal structure of photosystem II from *Synechococcus elongatus* at 3.8 Å resolution, *Nature*. 409 (2001) 739–743. doi:10.1038/35055589.
- [3] Y. Deawati, D. Onggo, I. Mulyani, I. Hastiawan, D. Kurnia, P. Lönnecke, S. Schmorl, B. Kersting, E. Hey-Hawkins, Synthesis, crystal structures, and superoxide dismutase activity of two new multinuclear manganese(III)-salen-4,4'-bipyridine complexes, *Inorganica Chim. Acta.* 482 (2018) 353–357. doi:10.1016/j.ica.2018.06.018.
- [4] A.B. Tomter, G. Zoppellaro, N.H. Andersen, H.P. Hersleth, M. Hammerstad, Å.K. Røhr, G.K. Sandvik, K.R. Strand, G.E. Nilsson, C.B. Bell, A.L. Barra, E. Blasco, L. Le Pape, E.I. Solomon, K.K. Andersson, Ribonucleotide reductase class I with different radical generating clusters, *Coord. Chem. Rev.* 257 (2013) 3–26. doi:10.1016/j.ccr.2012.05.021.
- [5] F. Fieschi, E. Torrents, L. Touloukhonova, A. Jordan, U. Hellman, J. Barbe, I. Gibert, M. Karlsson, B.M. Sjöberg, The manganese-containing ribonucleotide reductase of *Corynebacterium ammoniagenes* is a class Ib enzyme, *J. Biol. Chem.* 273 (1998) 4329–4337. doi:10.1074/jbc.273.8.4329.
- [6] D.W. Christianson, Structural chemistry and biology of manganese metalloenzymes, *Prog. Biophys. Mol. Biol.* 67 (1997) 217–243. doi:10.1016/S0079-6107(97)88477-5.
- [7] V.V. Barynin, P.D. Hempstead, A.A. Vagin, S.V. Antonyuk, W.R. Melik-Adamyanyan, V.S. Lamzin, P.M. Harrison, P.J. Artymiuk, The three-dimensional structure of the

- di-Mn catalase and the environment of the di-Mn sites in different redox states, *J. Inorg. Biochem.* 67 (1997) 196. doi:10.1016/S0162-0134(97)80071-2.
- [8] N. Sarkar, M. Das, S. Chattopadhyay, Two new manganese(III) complexes with salicylaldehyde Schiff bases: Synthesis, structure, self-assembly and phenoxazinone synthase mimicking activity, *Inorganica Chim. Acta.* 457 (2017) 19–28. doi:10.1016/j.ica.2016.11.009.
- [9] J. Cubillos, S. Vásquez, C. Montes de Correa, Salen manganese (III) complexes as catalysts for R-(+)-limonene oxidation, *Appl. Catal. A Gen.* 373 (2010) 57–65. doi:10.1016/j.apcata.2009.10.041.
- [10] Y. Noritake, N. Umezawa, N. Kato, T. Higuchi, Manganese Salen Complexes with Acid–Base Catalytic Auxiliary: Functional Mimetics of Catalase, *Inorg. Chem.* 52 (2013) 3653–3662. doi:10.1021/ic302101c.
- [11] A. Rezaeifard, M. Jafarpour, M.A. Nasser, R. Haddad, Pronounced Catalytic Activity of Manganese(III)- Schiff Base Complexes in the Oxidation of Alcohols by Tetrabutylammonium Peroxomonosulfate, *Helv. Chim. Acta.* 93 (2010) 711–717. doi:10.1002/hlca.200900262.
- [12] M.R. Bermejo, R. Carballido, M.I. Fernández-García, A.M. González-Noya, G. González-Riopedre, M. Maneiro, L. Rodríguez-Silva, Synthesis, Characterization, and Catalytic Studies of Mn(III)-Schiff Base-Dicyanamide Complexes: Checking the Rhombicity Effect in Peroxidase Studies, *J. Chem.* 2017 (2017) 1–10. doi:10.1155/2017/5465890.
- [13] H. Miyasaka, A. Saitoh, S. Abe, Magnetic assemblies based on Mn(III) salen analogues, *Coord. Chem. Rev.* 251 (2007) 2622–2664. doi:10.1016/j.ccr.2007.07.028.
- [14] H. Miyasaka, R. Clérac, T. Ishii, H.-C. Chang, S. Kitagawa, M. Yamashita, Out-of-plane dimers of Mn(III) quadridentate Schiff-base complexes with saltmen²⁻ and naphthmen²⁻ ligands: structure analysis and ferromagnetic exchange, *J. Chem. Soc. Dalt. Trans.* (2002) 1528–1534. doi:10.1039/b111094m.

- [15] H. Miyasaka, N. Matsumoto, H. Ōkawa, N. Re, E. Gallo, C. Floriani, Complexes Derived from the Reaction of Manganese(III) Schiff Base Complexes and Hexacyanoferrate(III): Syntheses, Multidimensional Network Structures, and Magnetic Properties, *J. Am. Chem. Soc.* 118 (1996) 981–994. doi:10.1021/ja952706c.
- [16] R. Bagai, G. Christou, The Drosophila of single-molecule magnetism: $[\text{Mn}_{12}\text{O}_{12}(\text{O}_2\text{CR})_{16}(\text{H}_2\text{O})_4]$, *Chem. Soc. Rev.* 38 (2009) 1011. doi:10.1039/b811963e.
- [17] C.-I. Yang, Z.-Z. Zhang, S.-B. Lin, A review of manganese-based molecular magnets and supramolecular architectures from phenolic oximes, *Coord. Chem. Rev.* 289–290 (2015) 289–314. doi:10.1016/j.ccr.2014.12.011.
- [18] S. Wang, Y.J. Li, F.F. Ju, W.T. Xu, K. Kagesawa, Y.H. Li, M. Yamashita, W. Huang, The molecular and supramolecular aspects in mononuclear manganese(III) Schiff-base spin crossover complexes, *Dalt. Trans.* 46 (2017) 11063–11077. doi:10.1039/c7dt01718a.
- [19] D. Villaman, C.J. McMonagle, M.R. Probert, O. Peña, Y. Moreno, M. Fuentealba, Structural studies of a manganese(III) complex with spin-crossover and thermochromic properties, *CrystEngComm.* 22 (2020) 3221–3233. doi:10.1039/c9ce01962f.
- [20] A. V. Tiunova, A. V. Kazakova, D. V. Korchagin, G. V. Shilov, S.M. Aldoshin, A.I. Dmitriev, M. V. Zhidkov, K. V. Zakharov, E.B. Yagubskii, Spin-Crossover and Slow Magnetic Relaxation Behavior in Hexachlororhenate(IV) Salts of Mn(III) Complexes $[\text{Mn}(5\text{-Hal-sal}_2\text{323})_2][\text{ReCl}_6]$ (Hal = Cl, Br), *Int. J. Mol. Sci.* 23 (2022) 11449. doi:10.3390/ijms231911449.
- [21] S. Realista, A.J. Fitzpatrick, G. Santos, L.P. Ferreira, S. Barroso, L.C.J. Pereira, N.A.G. Bandeira, P. Neugebauer, J. Hrubý, G.G. Morgan, J. Van Slageren, M.J. Calhorda, P.N. Martinho, A Mn(III) single ion magnet with tridentate Schiff-base ligands, *Dalt. Trans.* 45 (2016) 12301–12307. doi:10.1039/c6dt02538b.
- [22] A. Earnshaw, Introduction to magnetochemistry, Academic Press London and New York, 1968.

- [23] B.J. Kennedy, K.S. Murray, Magnetic properties and zero-field splitting in high-spin manganese(III) complexes. 1. Mononuclear and polynuclear Schiff-base chelates, *Inorg. Chem.* 24 (1985) 1552–1557. doi:10.1021/ic00204a029.
- [24] J. Krzystek, G.J. Yeagle, J.-H. Park, R.D. Britt, M.W. Meisel, L.-C. Brunel, J. Telser, High-Frequency and -Field EPR Spectroscopy of Tris(2,4-pentanedionato)manganese(III): Investigation of Solid-State versus Solution Jahn–Teller Effects, *Inorg. Chem.* 48 (2009) 3290–3290. doi:10.1021/ic900315h.
- [25] M. Dolai, A. Mondal, J.-L. Liu, M. Ali, Three novel mononuclear Mn(III)-based magnetic materials with square pyramidal versus octahedral geometries, *New J. Chem.* 41 (2017) 10890–10898. doi:10.1039/C7NJ02919E.
- [26] S. Naskar, S. Biswas, D. Mishra, B. Adhikary, L.R. Falvello, T. Soler, C.H. Schwalbe, S.K. Chattopadhyay, Studies on the relative stabilities of Mn(II) and Mn(III) in complexes with N_4O_2 donor environments: crystal structures of $[Mn(pybzhz)_2]$ and $[Mn(Ophsal)(imzH)_2]ClO_4$ (pybzhz = *N*-(benzoyl)-*N'*-(picolinylidene) hydrazine, Ophsal = *N,N'*-*o*-phenylenebis(salicylid), *Inorganica Chim. Acta.* 357 (2004) 4257–4264. doi:10.1016/j.ica.2004.06.018.
- [27] I. Syiemlieh, A. Kumar, S.D. Kurbah, A.K. De, R.A. Lal, Low-spin manganese(II) and high-spin manganese(III) complexes derived from disalicylaldehyde oxaloyldihydrazone: Synthesis, spectral characterization and electrochemical studies, *J. Mol. Struct.* 1151 (2018) 343–352. doi:10.1016/j.molstruc.2017.09.052.
- [28] D. Zhang, W. Lan, Z. Zhou, L. Yang, Q. Liu, Y. Bian, J. Jiang, Manganese(III) Porphyrin-Based Magnetic Materials, *Top. Curr. Chem.* 377 (2019) 18. doi:10.1007/s41061-019-0244-5.
- [29] P.-P. Liu, L. Sheng, X.-Q. Song, W.-Y. Xu, Y.-A. Liu, Synthesis, structure and magnetic properties of a new one dimensional manganese coordination polymer constructed by a new asymmetrical ligand, *Inorganica Chim. Acta.* 434 (2015) 252–257. doi:10.1016/j.ica.2015.05.026.
- [30] X.-Y. Liu, P.-P. Cen, L.-Z. Wu, F.-F. Li, W.-M. Song, G. Xie, S.-P. Chen, Tuning of Exchange Coupling and Switchable Magnetization Dynamics by Displacing the

- Bridging Ligands Observed in Two Dimeric Manganese(III) Compounds, *Sci. Rep.* 7 (2017) 44982. doi:10.1038/srep44982.
- [31] T. Birk, K.S. Pedersen, S. Piligkos, C.A. Thuesen, H. Weihe, J. Bendix, Magnetic Properties of a Manganese(III) Chain with Monoatomic Bridges: catena - MnF(salen), *Inorg. Chem.* 50 (2011) 5312–5314. doi:10.1021/ic2002699.
- [32] K. Das, A. Datta, B.B. Beyene, C. Massera, E. Garribba, C. Sinha, T. Akitsu, S. Tanka, A zig-zag end-to-end azido bridged Mn^{III} 1-D coordination polymer: Spectral elucidation, magnetism, redox study and biological activity, *Polyhedron.* 127 (2017) 315–322. doi:10.1016/j.poly.2017.02.017.
- [33] T.M. Ross, S.M. Neville, D.S. Innes, D.R. Turner, B. Moubaraki, K.S. Murray, Spin crossover in iron(III) Schiff-base 1-D chain complexes, *Dalt. Trans.* 39 (2010) 149–159. doi:10.1039/B913234A.
- [34] N. Novoa, T. Roisnel, P. Hamon, S. Kahlal, C. Manzur, H.M. Ngo, I. Ledoux-Rak, J.-Y. Saillard, D. Carrillo, J.-R. Hamon, Four-coordinate nickel(II) and copper(II) complex based ONO tridentate Schiff base ligands: synthesis, molecular structure, electrochemical, linear and nonlinear properties, and computational study, *Dalt. Trans.* 44 (2015) 18019–18037. doi:10.1039/C5DT02822A.
- [35] N. Novoa, C. Manzur, T. Roisnel, S. Kahlal, J.-Y. Saillard, D. Carrillo, J.-R. Hamon, Nickel(II)-Based Building Blocks with Schiff Base Derivatives: Experimental Insights and DFT Calculations, *Molecules.* 26 (2021) 5316. doi:10.3390/molecules26175316.
- [36] G. M. Sheldrick, SADABS, Program for Empirical Absorption Correction of Area Detector Data, (1996).
- [37] G.M. Sheldrick, SHELXT – Integrated space-group and crystal-structure determination, *Acta Crystallogr. Sect. A Found. Adv.* 71 (2015) 3–8. doi:10.1107/S2053273314026370.
- [38] G.M. Sheldrick, Crystal structure refinement with SHELXL, *Acta Crystallogr. Sect. C Struct. Chem.* 71 (2015) 3–8. doi:10.1107/S2053229614024218.

- [39] O. V Dolomanov, L.J. Bourhis, R.J. Gildea, J.A.K. Howard, H. Puschmann, OLEX2 : a complete structure solution, refinement and analysis program, *J. Appl. Crystallogr.* 42 (2009) 339–341. doi:10.1107/S0021889808042726.
- [40] M.A. Spackman, J.J. McKinnon, Fingerprinting intermolecular interactions in molecular crystals, *CrystEngComm.* 4 (2002) 378–392. doi:10.1039/B203191B.
- [41] J.J. McKinnon, D. Jayatilaka, M. a Spackman, Towards quantitative analysis of intermolecular interactions with Hirshfeld surfaces, *Chem. Commun.* 0 (2007) 3814. doi:10.1039/b704980c.
- [42] M.A. Spackman, D. Jayatilaka, Hirshfeld surface analysis, *CrystEngComm.* 11 (2009) 19–32. doi:10.1039/B818330A.
- [43] P.R. Spackman, M.J. Turner, J.J. McKinnon, S.K. Wolff, D.J. Grimwood, D. Jayatilaka, M.A. Spackman, CrystalExplorer : a program for Hirshfeld surface analysis, visualization and quantitative analysis of molecular crystals, *J. Appl. Crystallogr.* 54 (2021) 1006–1011. doi:10.1107/S1600576721002910.
- [44] C.F. Macrae, I.J. Bruno, J.A. Chisholm, P.R. Edgington, P. McCabe, E. Pidcock, L. Rodriguez-Monge, R. Taylor, J. van de Streek, P.A. Wood, Mercury CSD 2.0 – new features for the visualization and investigation of crystal structures, *J. Appl. Crystallogr.* 41 (2008) 466–470. doi:10.1107/S0021889807067908.
- [45] G.A. Bain, J.F. Berry, Diamagnetic Corrections and Pascal’s Constants, *J. Chem. Educ.* 85 (2008) 532. doi:10.1021/ed085p532.
- [46] C. Adamo, V. Barone, Toward reliable density functional methods without adjustable parameters: The PBE0 model, *J. Chem. Phys.* 110 (1999) 6158–6170. doi:10.1063/1.478522.
- [47] M. Ernzerhof, G.E. Scuseria, Assessment of the Perdew–Burke–Ernzerhof exchange–correlation functional, *J. Chem. Phys.* 110 (1999) 5029–5036. doi:10.1063/1.478401.
- [48] F. Weigend, R. Ahlrichs, Balanced basis sets of split valence, triple zeta valence and quadruple zeta valence quality for H to Rn: Design and assessment of accuracy,

- Phys. Chem. Chem. Phys. 7 (2005) 3297. doi:10.1039/b508541a.
- [49] M.H. Jamróz, Vibrational Energy Distribution Analysis (VEDA): Scopes and limitations, *Spectrochim. Acta Part A Mol. Biomol. Spectrosc.* 114 (2013) 220–230. doi:10.1016/j.saa.2013.05.096.
- [50] Chemcraft - graphical software for visualization of quantum chemistry computations, [Https://www.Chemcraftprog.Com](https://www.Chemcraftprog.Com).
- [51] R.E. Stratmann, G.E. Scuseria, M.J. Frisch, An efficient implementation of time-dependent density-functional theory for the calculation of excitation energies of large molecules, *J. Chem. Phys.* 109 (1998) 8218–8224. doi:10.1063/1.477483.
- [52] R. Bauernschmitt, R. Ahlrichs, Treatment of electronic excitations within the adiabatic approximation of time dependent density functional theory, *Chem. Phys. Lett.* 256 (1996) 454–464. doi:10.1016/0009-2614(96)00440-X.
- [53] M. Cossi, V. Barone, Time-dependent density functional theory for molecules in liquid solutions, *J. Chem. Phys.* 115 (2001) 4708–4717. doi:10.1063/1.1394921.
- [54] M. Cossi, G. Scalmani, N. Rega, V. Barone, New developments in the polarizable continuum model for quantum mechanical and classical calculations on molecules in solution, *J. Chem. Phys.* 117 (2002) 43–54. doi:10.1063/1.1480445.
- [55] F.H. Allen, O. Kennard, D.G. Watson, L. Brammer, A.G. Orpen, R. Taylor, Tables of bond lengths determined by X-ray and neutron diffraction. Part 1. Bond lengths in organic compounds, *J. Chem. Soc. Perkin Trans. 2.* (1987) S1. doi:10.1039/p298700000s1.
- [56] A.G. Orpen, L. Brammer, F.H. Allen, O. Kennard, D.G. Watson, R. Taylor, Supplement. Tables of bond lengths determined by X-ray and neutron diffraction. Part 2. Organometallic compounds and co-ordination complexes of the d- and f-block metals, *J. Chem. Soc. Dalton Trans.* 0 (1989) S1. doi:10.1039/dt98900000s1.
- [57] N. Novoa, F. Justaud, P. Hamon, T. Roisnel, O. Cador, B. Le Guennic, C. Manzur, D. Carrillo, J.-R. Hamon, Doubly phenoxide-bridged binuclear copper(II) complexes with one tridentate schiff base ligand: Synthesis, structural, magnetic and theoretical

- studies, *Polyhedron*. 86 (2015) 81–88. doi:10.1016/j.poly.2014.05.032.
- [58] G. Desiraju, T. Steiner, *The Weak Hydrogen Bond*, Oxford University Press, 2001. doi:10.1093/acprof:oso/9780198509707.001.0001.
- [59] P. Gilli, V. Bertolasi, V. Ferretti, G. Gilli, Evidence for intramolecular N-H...O resonance-assisted hydrogen bonding in β -enaminones and related heterodienes. A combined crystal-structural, IR and NMR spectroscopic, and quantum-mechanical investigation, *J. Am. Chem. Soc.* 122 (2000) 10405–10417. doi:10.1021/ja000921+.
- [60] V. Artigas, D. González, M. Fuentealba, Syntheses, characterisation and crystal structures of ferrocenyl β -diketones and their Schiff base NNO ligand derivatives with 2-picolylamine, *J. Mol. Struct.* 1129 (2017) 325–332. doi:10.1016/j.molstruc.2016.09.009.
- [61] Y.L. Feng, S.X. Liu, Chloro[*N,N'*-ethylenebis(3-imino-1-phenyl-1-butanonato-N,O)]manganese(III), [MnCl(C₂₂H₂₂N₂O₂)], *Acta Crystallogr. Sect. C Cryst. Struct. Commun.* 52 (1996) 2768–2770. doi:10.1107/S0108270196006579.
- [62] Y.-L. Feng, S.-X. Liu, Syntheses and characterization of three structure types for manganese(III) complexes with *N,N'*-ethylene bis (1-phenyl-3-imino-1-butanone), *J. Coord. Chem.* 44 (1998) 81–90. doi:10.1080/00958979808022882.
- [63] P. Guionneau, M. Marchivie, G. Bravic, J.-F. Létard, D. Chasseau, Co(II) molecular complexes as a reference for the spin crossover in Fe(II) analogues, *J. Mater. Chem.* 12 (2002) 2546–2551. doi:10.1039/B202610D.
- [64] J.K. McCusker, A.L. Rheingold, D.N. Hendrickson, Variable-Temperature Studies of Laser-Initiated $^5T_2 \rightarrow ^1A_1$ Intersystem Crossing in Spin-Crossover Complexes: Empirical Correlations between Activation Parameters and Ligand Structure in a Series of Polypyridyl Ferrous Complexes, *Inorg. Chem.* 35 (1996) 2100–2112. doi:10.1021/ic9507880.
- [65] R. Ohtani, A. Grosjean, R. Ishikawa, R. Yamamoto, M. Nakamura, J.K. Clegg, S. Hayami, Zero in-Plane Thermal Expansion in Guest-Tunable 2D Coordination Polymers, *Inorg. Chem.* 56 (2017) 6225–6233. doi:10.1021/acs.inorgchem.7b00282.

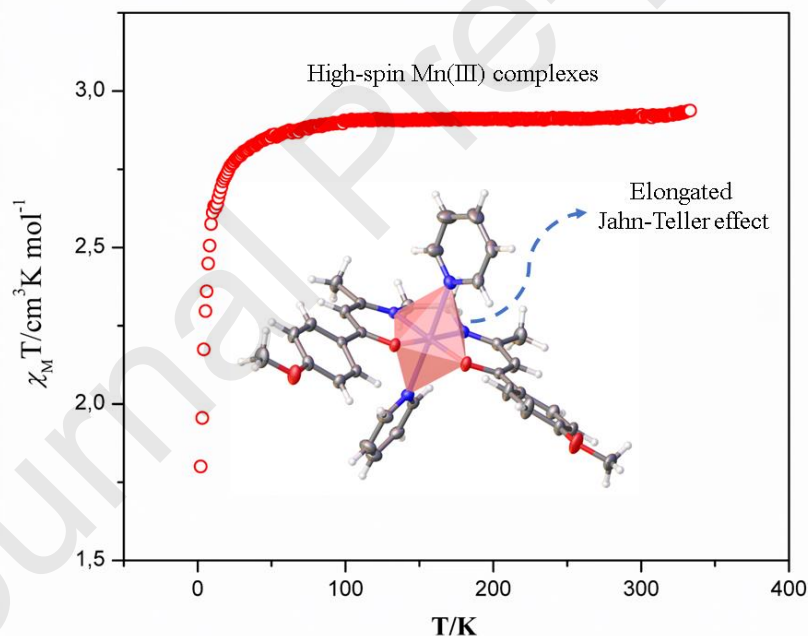
- [66] R. Ohtani, R. Yamamoto, H. Ohtsu, M. Kawano, J. Pirillo, Y. Hijikata, M. Sadakiyo, L.F. Lindoy, S. Hayami, Consecutive oxidative additions of iodine on undulating 2D coordination polymers: formation of I–Pt–I chains and inhomogeneous layers, *Dalt. Trans.* 48 (2019) 7198–7202. doi:10.1039/C8DT04624G.
- [67] S. Imatomi, R. Kitashima, T. Hamamastu, M. Okeda, Y. Ogawa, N. Matsumoto, One-dimensional Polynuclear Spin-crossover Iron(III) Complex Axially Bridged by 1,3-Bis(4-pyridyl)propane, *Chem. Lett.* 35 (2006) 502–503. doi:10.1246/cl.2006.502.
- [68] S. Imatomi, S. Hashimoto, N. Matsumoto, Inter- and Intrachain Spin-Transition Processes in One-Dimensional Polynuclear Iron(III) Complexes of *N,N'*-Ethylenebis(acetylacetylideneimine) Bridged by 1,3-Bis(4-pyridyl)propane and 1,4-Bis(imidazolyl)butane (*Eur. J. Inorg. Chem.* 6/2009), *Eur. J. Inorg. Chem.* 2009 (2009) 699–699. doi:10.1002/ejic.200990009.
- [69] R. Thakuria, N.K. Nath, B.K. Saha, The Nature and Applications of π – π Interactions: A Perspective, *Cryst. Growth Des.* 19 (2019) 523–528. doi:10.1021/acs.cgd.8b01630.
- [70] J. Lewiński, J. Zachara, I. Justyniak, M. Dranka, Hydrogen-bond supramolecular structure of group 13 Schiff base complexes, *Coord. Chem. Rev.* 249 (2005) 1185–1199. doi:10.1016/j.ccr.2004.11.013.
- [71] J. Meszko, K. Krzysiński, A. Konitz, J. Błażejowski, 2-Methylphenyl 2-methoxyacridine-9-carboxylate, *Acta Crystallogr. Sect. C Cryst. Struct. Commun.* 58 (2002) o157–o158. doi:10.1107/S0108270102000574.
- [72] J.. Kiss, K. Felföldi, I. Hannus, I. Pálinkó, Hydrogen bonded networks of methoxy-substituted α -phenylcinnamic acids studied by spectroscopic and computational methods, *J. Mol. Struct.* 565–566 (2001) 463–468. doi:10.1016/S0022-2860(00)00838-3.
- [73] J. Cisterna, M. Fuentealba, C. Manzur, D. Carrillo, Pentacoordinated Fe(III) complex containing the *cis*-N₂O₂ asymmetrical tetradentate Schiff base and *p*-Br-C₆H₄O- as ligands. Promising building block for the construction of dipolar D– π –A

- architectures: Synthesis, characterization, spectroscopic, electroche, J. Mol. Struct. 1228 (2021) 129709. doi:10.1016/j.molstruc.2020.129709.
- [74] J. Cisterna, V. Artigas, M. Fuentealba, C. Manzur, J.R. Hamon, D. Carrillo, Pentacoordinated isothiocyanate iron(III) complexes supported by asymmetric tetradentate donor and acceptor Schiff base ligands: Spectral, Structural and Hirshfeld Surface Analyses, J. Mol. Struct. 1230 (2021) 129864. doi:10.1016/j.molstruc.2020.129864.
- [75] N. Sarkar, K. Ghosh, R. González-Prieto, S. Herrero, S. Chattopadhyay, Construction of a new double phenoxo bridged asymmetric manganese(III) Schiff base complex: Observation of ferromagnetic interaction within the dimer and antiferromagnetic interaction between dimers, Polyhedron. 164 (2019) 138–145. doi:10.1016/j.poly.2019.01.061.
- [76] O. Kahn, Molecular Magnetism, VCH-Verlag, Weinheim, New York, 1993.
- [77] K. Mitra, S. Biswas, C.R. Lucas, B. Adhikary, Manganese(III) complexes of N₂O₂ donor 5-bromosalicylideneimine ligands: Combined effects of electron withdrawing substituents and chelate ring size variations on electrochemical properties, Inorganica Chim. Acta. 359 (2006) 1997–2003. doi:10.1016/j.ica.2006.01.013.
- [78] S. Biswas, K. Mitra, C.H. Schwalbe, C. Robert Lucas, S.K. Chattopadhyay, B. Adhikary, Synthesis and characterization of some Mn(II) and Mn(III) complexes of *N,N'*-*o*-phenylenebis(salicylideneimine)(LH₂) and *N,N'*-*o*-phenylenebis(5-bromosalicylideneimine)(L'H₂). Crystal structures of [Mn(L)(H₂O)(ClO₄)], [Mn(L)(NCS)] and an infinite linear chain, Inorganica Chim. Acta. 358 (2005) 2473–2481. doi:10.1016/j.ica.2005.01.026.
- [79] S. Biswas, K. Mitra, S.K. Chattopadhyay, B. Adhikary, C.R. Lucas, Mononuclear manganese(II) and manganese(III) complexes of N₂O donors involving amine and phenolate ligands: absorption spectra, electrochemistry and crystal structure of [Mn(L₃)₂](ClO₄), Transit. Met. Chem. 30 (2005) 393–398. doi:10.1007/s11243-004-7542-6.
- [80] S. Shova, A. Vlad, M. Cazacu, J. Krzystek, L. Bucinsky, M. Breza, D. Darvasiová,

P. Rapta, J. Cano, J. Telser, V.B. Arion, A five-coordinate manganese(III) complex of a salen type ligand with a positive axial anisotropy parameter D, *Dalt. Trans.* 46 (2017) 11817–11829. doi:10.1039/C7DT01809F.

Highlights

- Molecular and crystalline analysis of Mn(III) complexes
- DFT and TD-DFT studies for paramagnetic mononuclear complexes
- Noncommercial β -diketones for the synthesis of new tetradentate ligands



Credit authorship contribution statement

David Villaman: Methodology, software, writing and edition, original draft, supervision.
Walter A. Rabanal-León: Methodology and Software. **Mauricio Fuentealba:** Writing, review, edition, original draft, supervision. **Octavio Peña:** Methodology and review.
Yanko Moreno: Methodology and review.